Shape of the Hanle curve in spin-transport structures in the presence of an ac drive

R. C. Roundy,[1] M. C. Prestgard,[2] A. Tiwari,[2] and M. E. Raikh[1]

[1]*Department of Physics and Astronomy, University of Utah, Salt Lake City, Utah 84112, USA*
[2]*Department of Materials Science and Engineering, University of Utah, Salt Lake City, Utah 84112, USA*

Resistance between two ferromagnetic electrodes coupled to a normal channel depends on their relative magnetizations. The spin-dependent component, R, of the resistance changes with magnetic field, B, normal to the directions of magnetizations. In the field of spin transport, this change, $R(B)$, originating from the Larmour spin precession, is called the Hanle curve. We demonstrate that the shape of the Hanle curve evolves upon application of an ac drive and study this evolution theoretically as a function of the amplitude, B_1, and frequency, ω, of the drive. If the distance between the electrodes, L, is smaller than the spin-diffusion length, λ_s, the prime effect of a weak circular-polarized drive is the shift of the center of the curve to the value of B for which the Larmour frequency, ω_L, is $\sim B_1^2/\omega$. Magnetic resonance at $\omega_L \sim \omega$ manifests itself in the derivative, $\frac{dR}{dB}$. For large $L \gg \lambda_s$ the ac drive affects the Hanle curve if the drive amplitude exceeds the spin-relaxation rate, τ_s^{-1}, i.e., at $B_1\tau_s \gtrsim 1$. The prime effect of the drive is the elimination of a minimum in $R(B)$. A linearly polarized drive has a fundamentally different effect on the Hanle curve, affecting not its shape but rather its width.

I. INTRODUCTION

In the past decade there has been remarkable progress in the fabrication of lateral F-N-F structures (see Fig. 1) which exhibit spin transport. In the pioneering experiment Ref. [1] the existence of spin transport in an Al strip was demonstrated by measuring a voltage, V, generated between the strip and Co electrode upon injecting a current, I, through the other Co electrode. The sign of voltage could be reversed upon reversal of the relative magnetizations of the electrodes. Quantitative information about the spin transport was inferred from the dependence of the generated voltage on a weak external field, B, which caused the spin precession. In particular, it was observed that for the average spin precession angle $180°$ the generated voltage changes the sign.

A theory for the $\frac{V}{I} = R(B)$ dependence, i.e., for the Hanle profile, was first developed in Refs. [2,3]. Following Ref. [1], a concise derivation of the analytical result of Refs. [2,3] goes as follows. Suppose that the magnetizations of the injector and detector are directed along the x axis, while the field, B, is directed along the z axis. After a time, t, from the moment of injection the average x projection of spin of a given electron is $S_x(t) = e^{-t/\tau_s} \cos \omega_L t$, where $\omega_L = \gamma B$ is the Larmour frequency (γ is the gyromagnetic ratio) and τ_s is the spin-flip time in the nonmagnetic material. If the motion of the electron between the electrodes is a one-dimensional (1D) drift, then the times of arrival to the detector are distributed as $P(t) = \frac{1}{\sqrt{4\pi Dt}} \exp[-(L - v_d t)^2/4Dt]$. Here L is the distance between the electrodes (see Fig. 1), v_d is the drift velocity, and D is the diffusion coefficient. Then the nonlocal resistance, $R(B)$, is proportional $S_x(t)$ weighted with the distribution $P(t)$, i.e.,

$$R(B) = R_0 \int_0^\infty \frac{dt \cos(\omega_L t)}{\sqrt{4\pi Dt}} \exp\left[-\frac{t}{\tau_s} - \frac{(L - v_d t)^2}{4Dt}\right]. \quad (1)$$

The prefactor R_0 is B independent and is proportional to the product of polarizations of the injector and detector.

The integral Eq. (1) contains four parameters of the device: D, τ_s, L, and v_d. In fact, the B dependence of R is governed by only two dimensionless combinations: $\omega_L \tilde{\tau}_s$, where $\tilde{\tau}_s$ is the renormalized spin-flip time

$$\tilde{\tau}_s = \frac{\tau_s}{1 + \frac{v_0^2 \tau_s}{4D}}, \quad (2)$$

and the dimensionless length

$$\tilde{L} = \frac{L}{(4D\tilde{\tau}_s)^{1/2}}. \quad (3)$$

Besides, the integral can be evaluated analytically [1,7], and expressed in terms of the function $f(y)$ defined as

$$f(y) = \int_0^\infty \frac{ds}{s^{1/2}} \exp\left[-\frac{1}{s} - ys\right] = \left(\frac{\pi}{y}\right)^{1/2} \exp[-2y^{1/2}]. \quad (4)$$

Then the B dependence of the nonlocal resistance is simply given by

$$R(B) \propto f_r(y) = \mathrm{Re}\, f(y) = \left(\frac{\pi}{|y|}\right)^{1/2} \exp\left[-2|y|^{1/2} \cos\frac{\phi}{2}\right]$$
$$\times \cos\left(\frac{\phi}{2} + 2|y|^{1/2} \sin\frac{\phi}{2}\right), \quad (5)$$

where the absolute value, $|y|$, and the phase, ϕ, of the complex argument, y, are defined as

$$|y| = \tilde{L}^2\left(1 + \omega_L^2 \tilde{\tau}_s^2\right)^{1/2}, \quad \phi = \arctan(\omega_L \tilde{\tau}_s). \quad (6)$$

It follows from Eq. (5) that there are two characteristic shapes of the Hanle curve, loosely speaking, a short-device shape and a long-device shape. They are illustrated in Fig. 1.

With regard to experiments, Eq. (1) provides a remarkably accurate description of the Hanle curves measured in various spin-transport devices. Both shapes of $R(B)$ have been reported in many papers (see, e.g., Refs. [4–23]). Usually the value τ_s is inferred from $R(B)$, since $R(B)$ falls off at values $\omega_L \sim \tau_s^{-1}$. Experiments indicate that for the same structures, e.g., silicon based [4–8] or germanium based [9,10], the values of τ_s extracted from fitting the Hanle curves depend
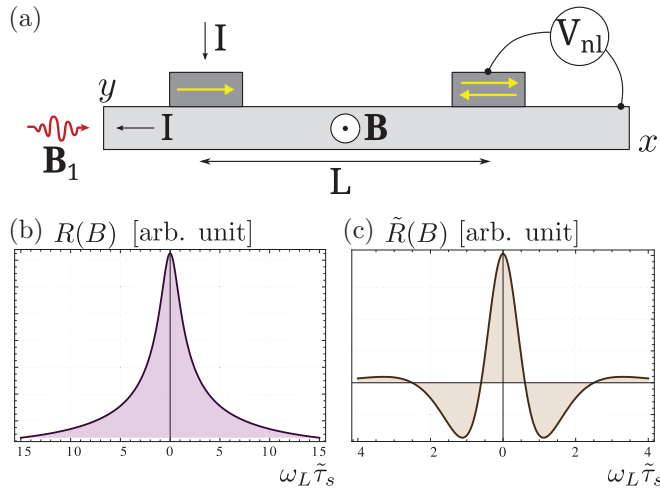
FIG. 1. (Color online) (a) Schematics of a standard spin-transport device. Nonlocal resistance is defined as a voltage between the channel and the right ferromagnet detector generated upon injecting the current through the left ferromagnetic electrode. While the polarized electrons travel diffusively the distance, L, their spin precesses in magnetic field, B, directed along the z axis. The driving ac field B_1 is either circularly polarized in the x-y plane or linearly polarized along x. The shapes of the Hanle curves in (b) short $L/\lambda_s = 0.1$ and (c) long, $L/\lambda_s = 2.4$, devices are calculated from Eq. (5).

strongly on the temperature and the doping level [24]. This strong dependence is also observed in the structures based on GaAs [11–15]. On the other hand, in graphene-based valves [16–20] the Hanle curves are broad or narrow depending on whether the graphene layers are exfoliated or epitaxially grown.

It should be noted that determination of *both* τ_s and the spin-diffusion length, $\lambda_s = (D\tau_s)^{1/2}$, from a single measured Hanle curve is somewhat ambiguous, in the sense that the same $R(B)$ can be very well fitted with two significantly different sets of τ_s and λ_s. To improve the accuracy of determination of these parameters in Ref. [12] the Hanle curves for several values of L were analyzed.

Overall, the excellent agreement of the experimentally measured Hanle profiles with theoretical prediction Eq. (5) seems surprising, since the theory is based on a rather crude description of the spin dynamics of injected carriers. For example, this description completely neglects the details of injection, such as geometry of electrodes. Modeling the transport as a purely 1D diffusion is also somewhat questionable [25,26]. On the other hand, a complete understanding of the domain of applicability and limitations of the drift-diffusion theory of spin transport seems crucial, since the contemporary research on inverse spin Hall effect [13,21,27–30] and its possible applications in the logic devices contains the drift-diffusion description at its core. One way of testing the drift-diffusion theory, which has already been realized experimentally [31,32], is to operate with spatially inhomogeneous spin-density profiles. For example, in Ref. [32] this profile was created using the interference of two laser beams.

In the present manuscript we suggest another "knob" to test the drift-diffusion theory. Namely, we demonstrate that

the Hanle profile can be manipulated by the ac drive. More specifically, we assume that, in addition to a static field B_0, an ac field in the x-y plane is applied. On general grounds, one can expect that the ac drive suppresses the $R(B)$ response by affecting the steady precession $S_x(t) = \cos \omega_L t$. It is also apparent that the drive should make the most pronounced effect on $R(B)$ if the drive frequency, ω, is comparable to $\tilde\omega_L$—the value corresponding to the width of the Hanle curve in the absence of the drive. For $\omega \gg \tilde\omega_L$ the ac field oscillates many times as an electron travels between the injector and detector, so that the effect of a weak drive with amplitude $\gamma B_1 \ll \omega$ averages out. It is somewhat unexpected that, in addition to a simple broadening, the drive gives rise to specific features in the shape of the Hanle curves.

Below we find and analyze the expression for $R(B)$ for an ac field with arbitrary amplitude and frequency for the case when it is circularly polarized. The prime effect is the shift of the center of $R(B)$ to the left or to the right depending on whether the polarization of the drive is left or right. We also analyze the evolution of the Hanle curves with increasing drive for the case when the drive is linearly polarized. In particular, we identify two peculiar regimes of the spin dynamics which are specific to linear polarization. They are realized when the drive is either very fast or very strong. We discuss how this dynamics manifests itself in the Hanle profile.

II. DYNAMICS OF THE LARMOUR SPIN PRECESSION IN THE PRESENCE OF THE AC DRIVE

To find the shape of the Hanle curve in the presence of the ac drive, $\boldsymbol{B}_1(t)$, it is necessary to solve the equation for the spin dynamics

$$\frac{d\boldsymbol{S}}{dt} + \gamma(\boldsymbol{B} + \boldsymbol{B}_1(t)) \times \boldsymbol{S} = 0 \qquad (7)$$

with initial conditions $S_x(0) = 1$, $S_y(0) = S_z(0) = 0$. Then the solution should be substituted into Eq. (1) instead of $\cos \omega_L t$. We assume that the external field is directed along z, i.e., $\boldsymbol{B} = B_0 \boldsymbol{k}$, while the ac field lies in the x-y plane. For this field we will consider the cases of circular and linear polarization separately.

A. Circular polarization

It is important that the components of the ac drive

$$B_x = B_1 \cos(\omega t + \varphi), \quad B_y = B_1 \sin(\omega t + \varphi) \qquad (8)$$

contain a random initial phase, φ. It emerges as a result of the randomness of the time moments at which electrons are injected from the electrode. The nonlocal resistance should be averaged over this phase.

For circular polarization the dynamics of the spin components can be found exactly, since in the rotating frame the ac field is static. We reproduce this textbook solution to track the random phase, φ, which leads to averaging out of certain contributions to $R(B)$.

In the rotating frame, $x' = x \cos \omega t + y \sin \omega t$, $y' = y \cos \omega t - x \sin \omega t$, the general solution of the Bloch equation

has the Rabi form

$$S'(t) = \left(S_0 - \frac{(H \cdot S_0)H}{H^2} \right) \cos \gamma H t$$
$$+ \frac{H \times S_0}{H} \sin \gamma H t + \frac{(H \cdot S_0)H}{H^2}, \qquad (9)$$

where the projections of the vector H, which is the effective magnetic field in the rotating frame, are defined as $H_{x'} = B_1 \cos \varphi$, $H_{y'} = B_1 \sin \varphi$, and $H_{z'} = B_0 - \frac{\omega}{\gamma}$. After implementing the initial condition $S_{x'}(0) = 1$ it is instructive to rewrite Eq. (9) in components:

$$S_{x'}(t) = \left(1 - \frac{B_1^2 \cos^2 \varphi}{B_1^2 + \left(B_0 - \frac{\omega}{\gamma} \right)^2} \right) \cos \gamma H t$$
$$+ \frac{B_1^2 \cos^2 \varphi}{B_1^2 + \left(B_0 - \frac{\omega}{\gamma} \right)^2},$$

$$S_{y'}(t) = \frac{B_1^2 \cos \varphi \sin \varphi}{B_1^2 + \left(B_0 - \frac{\omega}{\gamma} \right)^2} (1 - \cos \gamma H t)$$
$$+ \frac{B_0 - \frac{\omega}{\gamma}}{\sqrt{B_1^2 + \left(B_0 - \frac{\omega}{\gamma} \right)^2}} \sin \gamma H t,$$

$$S_{z'}(t) = -\frac{B_1 \left(B_0 - \frac{\omega}{\gamma} \right) \cos \varphi}{B_1^2 + \left(B_0 - \frac{\omega}{\gamma} \right)^2} (1 - \cos \gamma H t)$$
$$- \frac{B_1 \sin \varphi}{\sqrt{B_1^2 + \left(B_0 - \frac{\omega}{\gamma} \right)^2}} \sin \gamma H t. \qquad (10)$$

It is now seen from Eq. (10) that $S_{z'}$ vanishes after averaging and so does the first term in $S_{y'}$. In the remaining terms the averaging amounts to the replacement of $\cos^2 \varphi$ by $1/2$.

Going back to the laboratory system, $S_x = S_{x'} \cos \omega t - S_{y'} \sin \omega t$, $S_y = S_{y'} \cos \omega t + S_{x'} \sin \omega t$, we get

$$\langle S_x(t) \rangle = \frac{B_1^2}{2H^2} \cos \omega t + \frac{1}{2} \left(1 - \frac{B_1^2}{2H^2} + \frac{B_0 - \frac{\omega}{\gamma}}{H} \right)$$
$$\times \cos[(\gamma H + \omega)t] + \frac{1}{2} \left(1 - \frac{B_1^2}{2H^2} - \frac{B_0 - \frac{\omega}{\gamma}}{H} \right)$$
$$\times \cos[(\gamma H - \omega)t], \qquad (11)$$

$$\langle S_y(t) \rangle = \frac{B_1^2}{2H^2} \sin \omega t + \frac{1}{2} \left(1 - \frac{B_1^2}{2H^2} + \frac{B_0 - \frac{\omega}{\gamma}}{H} \right)$$
$$\times \sin[(\gamma H + \omega)t] - \frac{1}{2} \left(1 - \frac{B_1^2}{2H^2} - \frac{B_0 - \frac{\omega}{\gamma}}{H} \right)$$
$$\times \sin[(\gamma H - \omega)t]. \qquad (12)$$

We see that the averaged dynamics of S_x and S_y represents oscillations with driving frequency, ω, which are modulated by the "Rabi" envelope with frequency [33]

$$\gamma H = \sqrt{(\omega - \gamma B_0)^2 + (\gamma B_1)^2}. \qquad (13)$$

Thus, while the Rabi oscillations in $S_z(t)$ do not survive averaging over the initial phase, φ, they are still present in the

averaged dynamics of S_x and S_y. In the next section we study how this dynamics manifests itself in nonlocal resistance.

III. NONLOCAL RESISTANCE

Three contributions to S_x in Eq. (11) give rise to three terms in the nonlocal resistance, $R(B)$. It is convenient to express $R(B)$ through the same function, $f_r(y)$, which describes the Hanle shape in the absence of the drive and is defined by Eq. (4). One finds

$$R(B) \propto \left\{ \frac{B_1^2}{2H^2} f_r(y_\omega) + \frac{1}{2} \left(1 - \frac{B_1^2}{2H^2} + \frac{B_0 - \frac{\omega}{\gamma}}{H} \right) f_r(y_{\omega+\gamma H}) \right.$$
$$\left. + \frac{1}{2} \left(1 - \frac{B_1^2}{2H^2} - \frac{B_0 - \frac{\omega}{\gamma}}{H} \right) f_r(y_{-\omega+\gamma H}) \right\}. \qquad (14)$$

Here the arguments y_ω and $y_{\pm\omega+\gamma H}$ are defined by Eq. (6) with ω_L replaced by ω and $\pm\omega + \gamma H$, respectively. It is convenient to analyze the shape of the Hanle curves for short and long devices separately.

A. Small distance between the electrodes

In the limit of small $\tilde{L} \ll 1$ the function Eq. (5) for nonlocal resistance in the absence of the drive simplifies to

$$R(B) \propto \frac{\sqrt{\sqrt{1 + \omega_L^2 \tilde{\tau}_s^2} + 1}}{\sqrt{1 + \omega_L^2 \tilde{\tau}_s^2}} = \frac{\tilde{L}}{(2\pi)^{1/2}} f_r(\omega_L) \bigg|_{\tilde{L} \ll 1}. \qquad (15)$$

Naturally, it contains only a single scale $\omega_L \sim \tilde{\tau}_s^{-1}$.

If the magnetization of the injector is along the x axis while the magnetization of the detector is along the y axis, then the Hanle signal is proportional to $S_y(t)$. The corresponding expression for nonlocal resistance reads

$$\tilde{R}(B) \propto \left\{ \frac{B_1^2}{2H^2} f_i(y_\omega) + \frac{1}{2} \left(1 - \frac{B_1^2}{2H^2} + \frac{B_0 - \frac{\omega}{\gamma}}{H} \right) f_i(y_{\omega+\gamma H}) \right.$$
$$\left. - \frac{1}{2} \left(1 - \frac{B_1^2}{2H^2} - \frac{B_0 - \frac{\omega}{\gamma}}{H} \right) f_i(y_{-\omega+\gamma H}) \right\}, \qquad (16)$$

where the function $f_i(y)$ is defined through Eq. (5) as $\mathrm{Im} f(y)$, which amounts to the change of cosine by sine in the right-hand side. In the absence of the drive, the resistance $\tilde{R}(B)$ is an odd function of the magnetic field. In the limit of small $\tilde{L}$ it simplifies to

$$\tilde{R}(B) \propto \frac{\sqrt{\sqrt{1 + \omega_L^2 \tilde{\tau}_s^2} - 1}}{\sqrt{1 + \omega_L^2 \tilde{\tau}_s^2}} = \frac{\tilde{L}}{(2\pi)^{1/2}} f_i(\omega_L) \bigg|_{\tilde{L} \ll 1}. \qquad (17)$$

To find the shape of the Hanle curve in the presence of the drive, the asymptote Eq. (15) should be substituted into Eq. (14). In Fig. 2 we plot the modified Hanle curves calculated for the driving frequency $\omega\tilde{\tau}_s = 7$ and two magnitudes of the drive $\gamma B_1 \tilde{\tau}_s = 4$ and 6. We also plot the corresponding curves for $\tilde{R}(B)$. The chosen value of ω is so big because the full width at half maximum value of $R(B)$ in the absence of the drive is also big, approximately $4/\tilde{\tau}_s$. One can identify in Fig. 2 three major features caused by the drive.
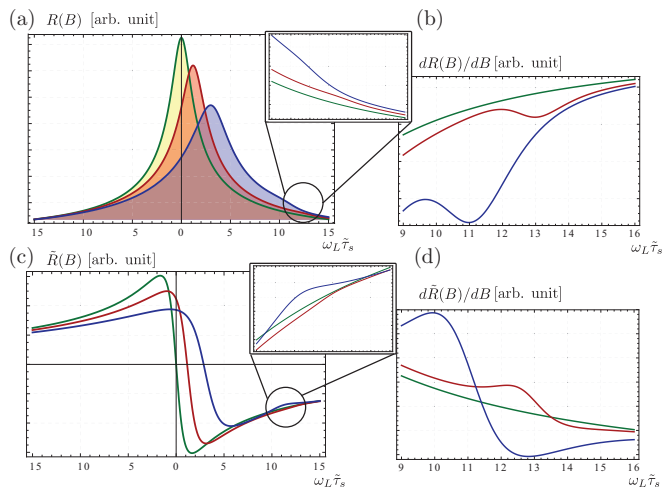
FIG. 2. (Color online) (a) Upon increasing the drive amplitude the Hanle curve broadens and its maximum is shifted quadratically with B_1. Green, red, and blue curves are plotted from Eq. (14) dimensionless drive frequency $\omega \tilde{\tau}_s = 7$ and three dimensionless drive amplitudes: $\gamma B_1 \tilde{\tau}_s = 0$ (green curve), 4 (red curve), and 6 (blue curve). Magnetic resonance $\omega_L = \omega$ resides around $\omega_L \tilde{\tau}_s = 11$. The corresponding region is enlarged. Magnetic resonance is pronounced in the dR/dB shown in (b); (c) and (d) are the same as (a) and (b) for the nonlocal resistance $\tilde{R}(B)$.

(i) The maximum shifts. The origin of this shift is the interplay of the prefactor and the function $f_r(y_{-\omega+\gamma H})$ in the third term of Eq. (14). First, this term gives the dominant contribution to $R(B)$ for small B_1. This is because the prefactor in the first term is $\propto B_1^2$, while the prefactor in the second term is $\propto B_1^4$ for $\omega_L < \omega$. On the other hand, the prefactor in the third term changes rapidly from one to zero at $\omega_L = \omega$. With regard to $f_r(y_{-\omega+\gamma H})$, it has two peaks at

$$\omega_L = \omega_{\pm} = \omega \pm \sqrt{\omega^2 - (\gamma B_1)^2}. \quad (18)$$

The peak at ω_+ is eliminated by the prefactor, while the peak at ω_-, which behaves as $(\gamma B_1)^2/2\omega$ at small B_1, survives and defines the position of the maximum in $R(B)$. For the two driving amplitudes plotted in Fig. 2 the expected shifts of the maxima are related as $9:4$, which is indeed the case.

(ii) The Hanle curves broaden with increasing the drive amplitude. Formally, this follows from the broadening of the steplike behavior of the prefactor in the third term with B_1.

(iii) Upon increasing B_1, the Hanle curves exhibit signatures of magnetic resonance. True magnetic resonance, $\omega_L = \omega$, is certainly present only in the dynamics of S_z. In the dynamics of S_x and S_y the manifestations of magnetic resonance are vague and originate from the fact that the derivative of the arguments $\omega \pm \gamma H$ with respect to B is equal to $(\omega \pm \gamma B_0)/\gamma H$. It passes through zero at the magnetic-resonance condition and changes rapidly from -1 to 1 in its vicinity. This change translates into a kinklike behavior indicated in Fig. 2. More pronounced signatures of the magnetic resonance can be seen in the derivative dR/dB, also shown in Fig. 2. The derivative develops a plateau.
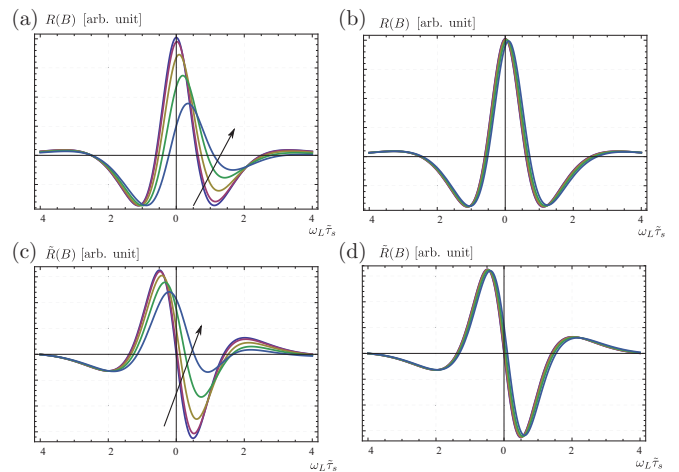

FIG. 3. (Color online) (a) In a spin-transport device with a long channel the prime effect of the ac drive on the Hanle curve is elimination of a minimum. The $R(B)$ curves are plotted from Eq. (14) for $L/\lambda_s = 2.4$, $\omega \tilde{\tau}_s = 1.1$, and five values of the driving field $\gamma B_1 \tilde{\tau}_s = 0$, 0.25, 0.5, 0.75, and 1. Black arrow shows the direction in which γB_1 increases. (b) Same curves as (a) but for the high-frequency drive, $\omega \tilde{\tau}_s = 5$, show a weak response to the drive. (c) and (d) are the same as (a) and (b) for $\tilde{R}(B)$.

The shapes of $\tilde{R}(B)$ shown in Fig. 2 evolve with the drive in a predictable fashion. Namely, the position of zero shifts to a finite magnetic field $\sim (\gamma B_1)^2/2\omega$ and the curves broaden. The signatures of magnetic resonance are more pronounced in $\tilde{R}(B)$. As seen in Fig. 2 the derivative $d\tilde{R}/dB$ exhibits a jumplike behavior near $\omega_L = \omega$.

B. The injector and the detector are far apart

In a long device, $\tilde{L} \gg 1$, the nonlocal resistance Eq. (5) exhibits oscillations decaying with the magnetic field. First, two zeros correspond to magnetic fields $\omega_L \tilde{\tau}_s \approx \pi/2\tilde{L}$ and $3\pi/2\tilde{L}$. The effect of the ac drive on $R(B)$ is most pronounced when the driving frequency lies between these two values. This is illustrated in Fig. 3. Two sets of curves in Fig. 3 correspond to the same values of the drive amplitudes but to different driving frequencies. In the left and right sets the frequencies differ by a factor of 5. It is seen that the Hanle shapes in the right set do not respond to the drive. The reason for that is that the value $\omega \tilde{\tau}_s$ for this set is 5, which is much bigger than $\pi/\tilde{L} \approx 1.4$. For the left set, $\omega \tilde{\tau}_s = 1.1$, which is close to $\pi/\tilde{L}$. The lively response of $R(B)$ and $\tilde{R}(B)$ to the drive at this frequency originates from the fact that a nondriven curve is flat around $\omega_L \tilde{\tau}_s \approx 1.2$. With the choice $\omega \tilde{\tau}_s = 1.1$ this ω_L is near magnetic resonance and the fast change of the prefactors in Eq. (14) with ω_L is not overshadowed by the change of the function $f_r(y)$.

IV. LINEAR POLARIZATION OF THE DRIVE

The expressions for nonlocal resistance obtained in the previous section are exact, in the sense that they apply at arbitrary strengths and frequencies of the circularly polarized drive. We analyzed them for the situation when both γB_1 and ω are comparable to the width of the Hanle curve. It is easy
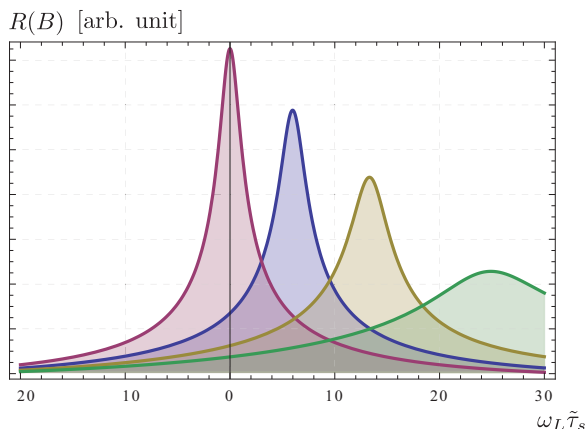
FIG. 4. (Color online) Evolution of the Hanle curves in a short device with increasing the amplitude of the drive and very high driving frequency, $\omega\tilde{\tau}_s = 30$. The curves are plotted from Eq. (14) for the values of $\gamma B_1\tilde{\tau}_s = 0$ (magenta), 18 (blue), 25 (tan), and 30 (green). The prime effect of the drive is the shift of the maximum with slow broadening of the shape.

to see from Eq. (14) what happens to the Hanle curve when both γB_1 and ω are much bigger than γB_0. With the shape of the Hanle curve dominated by the third term in Eq. (14), the argument $-\omega + \gamma H$ of f_r in this term can, at low B_0, be expanded as

$$-\omega + \gamma H \approx -\omega + [(\gamma B_1)^2 + \omega^2]^{1/2} - \frac{\gamma B_0\omega}{[(\gamma B_1)^2 + \omega^2]^{1/2}}.$$

$$(19)$$

Equation (19) suggests that under a fast and strong circularly polarized drive the Hanle curve simply shifts to the right, preserving its shape. This is illustrated in Fig. 4, where the $R(B)$ curves are plotted from Eq. (14) for fast and strong drives. We intentionally chose a very high driving frequency $\omega\tilde{\tau}_s = 30$ to allow the $R(B)$ peak to shift substantially with increasing $\gamma B_1\tilde{\tau}_s$.

Obviously, under a linearly polarized drive, the $R(B)$ dependence maintains its symmetry with respect to $B = 0$. From Fig. 4 one would expect that, when the maximum of $R(B)$ for the circularly polarized drive is shifted by more than the width in the absence of the drive, then the effect of the linearly polarized drive would be a "symmetrized" peak. This is, actually, not the case. The reason is that the spin dynamics for a fast linearly polarized and circularly polarized drives are very different.

Assume that the driving field oscillates along the x axis, $\mathbf{B}_1(t) = \mathbf{i}B_1\cos(\omega t + \varphi)$. In the Appendix we derive the following expressions for the dynamics of the spin projections averaged over φ:

$$\langle S_x(t)\rangle = \cos\left[\gamma B_0 J_0\left(\frac{\gamma B_1}{\omega}\right)t\right], \qquad (20)$$

$$\langle S_y(t)\rangle = J_0\left(\frac{\gamma B_1}{\omega}\right)\sin\left[\gamma B_0 J_0\left(\frac{\gamma B_1}{\omega}\right)t\right], \qquad (21)$$

$$\langle S_z(t)\rangle = 0. \qquad (22)$$

The above result leads us to the conclusion that, with the fast linearly polarized drive, the curves $R(B)$ and $\tilde{R}(B)$ have exactly the same shape as in the absence of the drive. The only difference is that the Larmour frequency ω_L gets replaced by $\omega_L J_0(\gamma B_1/\omega)$, signifying the broadening of the curves, which *oscillates* with the drive amplitude.

A. Strong drive

Another regime of the spin dynamics specific for a linearly polarized drive is realized when the drive is very strong, $B_1 \gg B_0$. We will describe this regime qualitatively. As $\mathbf{B}_1(t)$ oscillates, it exceeds the static field B_0 during, practically, the entire period, $2\pi/\omega$. Then B_0 has a negligible effect on the spin dynamics. However, during short-time intervals, δt, when $\mathbf{B}_1(t)$ passes through zero, the electron spin is affected by B_0 only. During each of these intervals the spin rotates by the angle $\sim B_0\delta t$. Thus, the net rotation after time t is $\sim(B_0\delta t)\omega t$. Now the value δt can be estimated from the relation $B_1(\omega\delta t) = B_0$. This leads us to the conclusion that the spin dynamics, averaged over the the period of the drive, is still a regular spin precession around the z axis but with effective frequency $\sim\gamma B_0^2/B_1$ instead of ω_L. One consequence of the replacement of ω_L by $\gamma B_0^2/B_1 \ll \omega_L$ in Eq. (5) is a general broadening of the Hanle profile, which can be controlled by the strength of the drive. The other consequence is that the Hanle profile acquires a flat top.

V. DISCUSSION

Our overall conclusion is that the ac drive with frequency ω affects nonlocal spin transport if its amplitude is strong enough, $\gamma B_1 \gtrsim (\frac{\omega}{\tilde{\tau}_s})^{-1/2}$. Choosing for an estimate the values $\tau_s = 50$ ns and $\omega = 200$ MHz, we find that the driving amplitude must be bigger than 1 mT to affect the spin transport. This value is quite realistic for experiments where the effects of the ac drive are studied by electrical measurements [35].

Our consideration is based on the conventional model of spin transport which is captured by Eq. (1) for nonlocal resistance. This implicitly suggests that all the physical assumptions underlying this model are met. For example, it assumed that the the resistance of the channel is much smaller than the contact resistance at the boundary with ferromagnets. It is also assumed that the resistance Eq. (1) is *ohmic*, i.e., the deviation from the local charge neutrality is completely neglected. This deviation would necessitate simultaneous solution of the Poisson and drift-diffusion equations in a self-consistent manner [36,37]. We have also disregarded the magnetic proximity effects at the F-N interfaces, which can be important if the normal channel is graphene [38].

In this paper we considered the domain of parameters $\gamma B_1 < \omega$ and found that modification of the shapes of the Hanle curves is primarily the broadening and the shift of the maximum. The above numerical estimate suggests that the opposite relation $\gamma B_1 > \omega$ is also experimentally accessible. For this domain of a strong circularly polarized drive the shapes of the Hanle curves change dramatically, as it is illustrated in Fig. 5. The curves exhibit *two* scales, which can be qualitatively
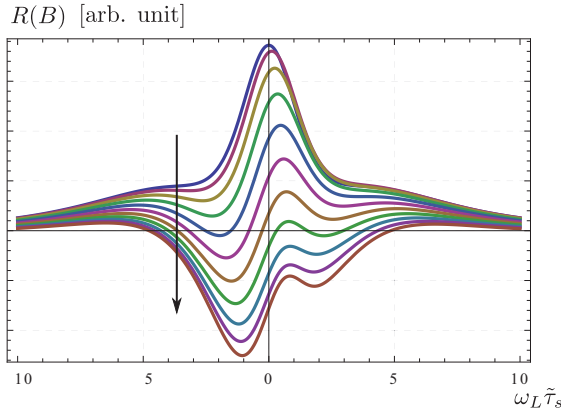
FIG. 5. (Color online) At strong drive $\gamma B_1 > \omega$. The zero-drive Hanle curves not only lose their symmetry but acquire additional maxima and minima. The evolution of the Hanle shapes for a given $\gamma B_1 \tilde{\tau}_s = 2$ and $L/\lambda_s = 1.4$ is plotted from Eq. (14) for driving frequencies $\omega \tilde{\tau}_s$ taking the values between zero and one with a step 0.1. The arrow shows the direction of the increase of the driving frequency.

interpreted as follows. The low-B scale is the signature of the condition $\omega_L = \omega$ for which the argument $y_{-\omega+\gamma H}$ of f_r in Eq. (14) is minimal. The high-B feature is the signature of $\omega_L = \gamma B_1$ at which the prefactor in the third term in Eq. (14) changes significantly.

One of our main findings is that the fast and strong circularly polarized ac fields affect the Hanle profile dramatically, as illustrated in Fig. 4, while the linearly polarized field with the same amplitude and frequency has a little effect on the Hanle curve. This is in contrast to usual reasoning in magnetic resonance suggesting to treat the linear polarization as the superposition of two circular polarizations and keep only the polarization which corotates with precessing electron spin. The easiest way to understand the difference between the spin dynamics for linear and circular polarizations qualitatively is to set B_0 equal to zero. Then, with initial spin direction along x, the ac field, linearly polarized along x, would not cause any spin dynamics *at all*. On the other hand, according to Eqs. (11) and (12), the average spin will precess around the z axis (if $\gamma B_1 \ll \omega$) even when $B_0 = 0$.

The effect of the ac drive on the Hanle curve is more pronounced for circular polarization of the drive when the symmetry of the curve is broken. In experiment, the circular polarization of microwaves is achieved [39–41] with the help of two crossed microstrip resonators. In particular, in Ref. [40] it was demonstrated that the optically detected magnetic resonance spectrum of the nitrogen vacancies in diamond depends on the direction of the circular polarization of microwaves.

Sensitivity of the Hanle curves to the ac drive can serve as a test of whether a spin-polarized current indeed flows through the channel of the device. Such a test is especially important for three-terminal devices [8,42–47] where the question about the spin injection is still controversial. In these devices, with only one of the electrodes being a ferromagnet, the spin-dependent buildup of a voltage between the injector and detector observed in experiment, as well as

the sensitivity of this voltage to the magnetic field [8,42,43], can be caused by the physical mechanisms [44–47], which are quite different from the conventional drift-diffusion picture. Definitely the sensitivities of "drift-diffusion" magnetoresistance to the ac drive, studied in the present paper, and the magnetoresistance within the recent models [44–47] are very different.

APPENDIX

The equations of motion for the spin projections in the presence of the linearly polarized drive, $\mathbf{B}_1(t) = \mathbf{i}B_1 \cos(\omega t + \varphi)$, assume the form

$$\frac{dS_x}{dt} = -\gamma B_0 S_y, \tag{A1}$$

$$\frac{dS_y}{dt} = \gamma B_0 S_x - \gamma B_1 S_z \cos \omega t, \tag{A2}$$

$$\frac{dS_z}{dt} = \gamma B_1 S_y \cos \omega t. \tag{A3}$$

To handle the fast linearly polarized drive it is convenient [34] to switch to the variables

$$S_{x'} = S_x, \tag{A4}$$

$$S_{y'} = S_y \cos \theta(t) + S_z \sin \theta(t), \tag{A5}$$

$$S_{z'} = -S_y \sin \theta(t) + S_z \cos \theta(t), \tag{A6}$$

where the angle $\theta(t)$ is defined as

$$\theta(t) = \frac{\gamma B_1}{\omega} \sin(\omega t + \varphi). \tag{A7}$$

The physical meaning of the above transformation is moving into the frame rotating around the ac field; the ac field is "canceled" in the new frame. The equations of motion for the new variables read

$$\frac{dS_{x'}}{dt} = \gamma B_0 S_{z'} \sin \theta(t) - \gamma B_0 S_{y'} \cos \theta(t), \tag{A8}$$

$$\frac{dS_{y'}}{dt} = \gamma B_0 S_{x'} \cos \theta(t), \tag{A9}$$

$$\frac{dS_{z'}}{dt} = -\gamma B_0 S_{x'} \sin \theta(t). \tag{A10}$$

One can see that there are two natural frequencies in the system Eq. (A8): one is γB_0 and the other is ω. Since the second frequency is much bigger than the first, we can average the equations over time interval $(-\frac{\pi}{\omega}, \frac{\pi}{\omega})$ assuming that the spin projections do not change significantly during this interval. Taking into account that $\langle \cos(\theta) \rangle = J_0(\gamma B_1/\omega)$, where $J_0(z)$

is a zero-order Bessel function, we get

$$\frac{dS_{x'}}{dt} = -\gamma B_0 J_0\left(\frac{\gamma B_1}{\omega}\right)S_{y'}, \tag{A11}$$

$$\frac{dS_{y'}}{dt} = \gamma B_0 J_0\left(\frac{\gamma B_1}{\omega}\right)S_{x'}, \tag{A12}$$

$$\frac{dS_{z'}}{dt} = 0. \tag{A13}$$

We see that the dynamics after averaging is slow, which justifies the averaging performed [34]. Upon returning to the laboratory frame the solution of the system Eq. (A11) satisfying

the condition $S_x(0) = 1$ reads

$$S_x(t) = \cos\left[\gamma B_0 J_0\left(\frac{\gamma B_1}{\omega}\right)t\right], \tag{A14}$$

$$S_y(t) = \sin\left[\gamma B_0 J_0\left(\frac{\gamma B_1}{\omega}\right)t\right]\cos\left[\frac{\gamma B_1}{\omega}\sin(\omega t + \varphi)\right], \tag{A15}$$

$$S_z(t) = \sin\left[\gamma B_0 J_0\left(\frac{\gamma B_1}{\omega}\right)t\right]\sin\left[\frac{\gamma B_1}{\omega}\sin(\omega t + \varphi)\right]. \tag{A16}$$

As a final step, we average over the initial phase, φ, and arrive to Eq. (20).

[1] F. J. Jedema, A. T. Filip, and B. J. van Wees, Nature (London) **410**, 345 (2001).

[2] M. Johnson and R. H. Silsbee, Phys. Lett. **55**, 1790 (1985).

[3] M. Johnson and R. H. Silsbee, Phys. Rev. B **37**, 5312 (1988).

[4] I. Appelbaum, B. Huang, and D. Monsma, Nature (London) **447**, 295 (2007).

[5] B. Huang and I. Appelbaum, Phys. Rev. B **77**, 165331 (2008).

[6] J. Li, B. Huang, and I. Appelbaum, Appl. Phys. Lett. **92**, 142507 (2008); B. Huang, H.-J. Jang, and I. Appelbaum, *ibid.* **93**, 162508 (2008).

[7] T. Sasaki, T. Oikawa, T. Suzuki, M. Shiraishi, Y. Suzuki, and K. Noguchi, IEEE Trans. Magn. **46**, 1436 (2010).

[8] Y. Aoki, M. Kameno, Y. Ando, E. Shikoh, Y. Suzuki, T. Shinjo, M. Shiraishi, T. Sasaki, T. Oikawa, and T. Suzuki, Phys. Rev. B **86**, 081201(R) (2012).

[9] L.-T. Chang, W. Han, Y. Zhou, J. Tang, I. A. Fischer, M. Oehme, J. Schulze, R. K. Kawakami, and K. L. Wang, Semicond. Sci. Technol. **28**, 015018 (2013).

[10] K. Kasahara, Y. Fujita, S. Yamada, K. Sawano, M. Miyao, and K. Hamaya, Appl. Phys. Express **7**, 033002 (2014).

[11] S. A. Crooker, M. Furis, X. Lou, C. Adelmann, D. L. Smith, C. J. Palmstrøm, and P. A. Crowell, Science **309**, 2191 (2005).

[12] X. Lou, C. Adelmann, S. A. Crooker, E. S. Garlid, J. Zhang, S. M. Reddy, S. D. Flexner, C. J. Palmstrøm, and P. A. Crowell, Nat. Phys. **3**, 197 (2007).

[13] K. Olejník, J. Wunderlich, A. C. Irvine, R. P. Campion, V. P. Amin, J. Sinova, and T. Jungwirth, Phys. Rev. Lett. **109**, 076601 (2012).

[14] S. Majumder, B. Kardasz, G. Kirczenow, A. S. Thorpe, and K. L. Kavanagh, Semicond. Sci. Technol. **28**, 035003 (2013).

[15] J. Misuraca, J.-I. Kim, J. Lu, K. Meng, L. Chen, X. Yu, J. Zhao, P. Xiong, and S. von Molnár, Appl. Phys. Lett. **104**, 082405 (2014).

[16] N. Tombros, C. Jozsa, M. Popinciuc, H. T. Jonkman, and B. J. van Wees, Nature (London) **448**, 571 (2007).

[17] C. Józsa, M. Popinciuc, N. Tombros, H. T. Jonkman, and B. J. van Wees, Phys. Rev. Lett. **100**, 236603 (2008); Phys. Rev. B **79**, 081402 (2009).

[18] M. H. D. Guimarães, A. Veligura, P. J. Zomer, T. Maassen, I. J. Vera-Marun, N. Tombros, and B. J. van Wees, Nano Lett. **12**, 3512 (2012).

[19] T. Yamaguchi, Y. Inoue, S. Masubuchi, S. Morikawa, M. Onuki, K. Watanabe, T. Taniguchi, R. Moriya, and T. Machida, Appl. Phys. Express **6**, 073001 (2013).

[20] A. Dankert, M. V. Kamalakar, J. Bergsten, and S. P. Dash, Appl. Phys. Lett. **104**, 192403 (2014).

[21] E. S. Garlid, Q. O. Hu, M. K. Chan, C. J. Palmstrøm, and P. A. Crowell, Phys. Rev. Lett. **105**, 156602 (2010).

[22] S. Kuhlen, K. Schmalbuch, M. Hagedorn, P. Schlammes, M. Patt, M. Lepsa, G. Güntherodt, and B. Beschoten, Phys. Rev. Lett. **109**, 146603 (2012).

[23] S. Jahangir, F. Doğan, H. Kum, A. Manchon, and P. Bhattacharya, Phys. Rev. B **86**, 035315 (2012).

[24] I. Žutić, J. Fabian, and S. Das Sarma, Rev. Mod. Phys. **76**, 323 (2004).

[25] H. Dery, Ł. Cywiński, and L. J. Sham, Phys. Rev. B **73**, 041306(R) (2006).

[26] M. Johnson and R. H. Silsbee, Phys. Rev. B **76**, 153107 (2007).

[27] Y. Niimi, Y. Kawanishi, D. H. Wei, C. Deranlot, H. X. Yang, M. Chshiev, T. Valet, A. Fert, and Y. Otani, Phys. Rev. Lett. **109**, 156602 (2012).

[28] Y. Niimi, H. Suzuki, Y. Kawanishi, Y. Omori, T. Valet, A. Fert, and Y. Otani, Phys. Rev. B **89**, 054401 (2014).

[29] S. Watanabe, K. Ando, K. Kang, S. Mooser, Y. Vaynzof, H. Kurebayashi, E. Saitoh, and H. Sirringhaus, Nat. Phys. **10**, 308 (2014).

[30] M. C. Prestgard and A. Tiwari, Appl. Phys. Lett. **104**, 122402 (2014).

[31] Y. Manzke, R. Farshchi, P. Bruski, J. Herfort, and M. Ramsteiner, Phys. Rev. B **87**, 134415 (2013).

[32] G. Wang, B. L. Liu, A. Balocchi, P. Renucci, C. R. Zhu, T. Amand, C. Fontaine, and X. Marie, Nat. Commun. **4**, 2372 (2013).

[33] I. I. Rabi, Phys. Rev. **51**, 652 (1937).

[34] R. Glenn, M. E. Limes, B. Pankovich, B. Saam, and M. E. Raikh, Phys. Rev. B **87**, 155128 (2013).

[35] D. R. McCamey, K. J. van Schooten, W. J. Baker, S.-Y. Lee, S.-Y. Paik, J. M. Lupton, and C. Boehme, Phys. Rev. Lett. **104**, 017601 (2010).

[36] I. Žutić, J. Fabian, and S. Das Sarma, Phys. Rev. B **64**, 121201 (2001).

[37] I. Žutić, J. Fabian, and S. Das Sarma, Phys. Rev. Lett. **88**, 066603 (2002).

[38] P. Lazić, G. M. Sipahi, R. K. Kawakami, and I. Žutić, Phys. Rev. B **90**, 085429 (2014).

[39] T. P. M. Alegre, A. C. Torrezan, and G. Medeiros-Ribeiro, Appl. Phys. Lett. **91**, 204103 (2007).

[40] T. P. M. Alegre, C. Santori, G. Medeiros-Ribeiro, and R. G. Beausoleil, Phys. Rev. B **76**, 165205 (2007).

[41] J. J. Henderson, C. M. Ramsey, H. M. Quddusi, and E. d. Barco, Rev. Sci. Instrum. **79**, 074704 (2008).

[42] S. J. Dash, S. Sharma, R. S. Patel, M. P. de Jong, and R. Jansen, Nature (London) **462**, 491 (2009).

[43] K. R. Jeon, B. C. Min, I. J. Shin, C. Y. Park, H. S. Lee, Y. H. Jo, and S. C. Shin, Appl. Phys. Lett. **98**, 262102 (2011).

[44] Y. Song and H. Dery, Phys. Rev. Lett. **113**, 047205 (2014).

[45] H. N. Tinkey, P. Li, and I. Appelbaum, Appl. Phys. Lett. **104**, 232410 (2014).

[46] A. G. Swartz, S. Harashima, Y. Xie, D. Lu, B. Kim, C. Bell, Y. Hikita, and H. Y. Hwang, Appl. Phys. Lett. **105**, 032406 (2014).

[47] O. Txoperena, Y. Song, L. Qing, M. Gobbi, L. E. Hueso, H. Dery, and F. Casanova, Phys. Rev. Lett. **113**, 146601 (2014).